Numerical simulation of single- and multi-step shear stress relaxations of isotropic magnetorheological elastomer using fractional derivative viscoelastic models

T. H. NAM, I. PETRÍKOVÁ, B. MARVALOVÁ

Department of Applied Mechanics, Faculty of Mechanical Engineering,
Technical University of Liberec, Studentská 1402/2, 461 17 Liberec 1, Czech Republic,
e-mails: thnam.hut@gmail.com, nam.tran.huu@tul.cz

THE PAPER PRESENTS NUMERICAL SIMULATIONS of single- and multi-step shear stress relaxations of isotropic magnetorheological elastomer (MRE) using fractional derivative Maxwell and Kelvin–Voigt viscoelastic models. The isotropic MRE has been fabricated by filling micro-sized carbonyl iron particles in silicone rubber. Fractional derivative Maxwell and Kelvin–Voigt viscoelastic models were used to fit the experimental data of the isotropic MRE measured by single- and multi-step relaxation tests at different constant strains and external magnetic fields. The fractional Maxwell viscoelastic model showed a relatively large difference between the measured and calculated results. The fractional Kelvin–Voigt model was fitted well with the experimental data of the isotropic MRE at various constant strain levels under different magnetic fields in both single- and multi-step shear stress relaxations. The calculated shear stress with the long-term prediction is in excellent agreement with the measured one. Therefore, the fractional derivative Kelvin–Voigt viscoelastic model is applicable to predict the long-term stress relaxation of the isotropic MRE.

Key words: magnetorheological elastomer, stress relaxation, fractional viscoelastic model, magnetic field.

1. Introduction

MAGNETORHEOLOGICAL ELASTOMERS (MREs), described by RIGBI and JILKEN in 1983 [1], are an emerging class of intelligent materials because they are capable of changing their shape, mechanical characteristic, and damping properties in the presence of a magnetic field [2]. MREs have been prepared by filling magnetizable particles in non-magnetic polymer matrices. They exhibit changes in their shape, rheological, viscoelastic, and damping properties under an external magnetic field [3]. MREs have been potential applications in vibration absorbers and isolators [4–7], sensors and actuators [8, 9], engine mounts for automobiles [10], peristaltic pumps [11], metamaterials [12, 13], shape-morphing structures [14], and soft robotics [15]. Therefore, the research on the time-dependent viscoelastic properties of MREs is essential for real engineering applications.

Among the time-dependent mechanical properties of viscoelastic polymeric materials, stress relaxation has been extensively studied by experimental and numerical methods. The simple shear and compression stress relaxations of filled natural rubbers were presented by AMIN et al. [16]. Besides, the simple compressive stress relaxation behavior of filled rubber composites in tensile and compression regimes was studied by WANG and HAN [17]. The shear stress relaxation response of MRE based on the polyurethane/epoxy interpenetrating polymer networks matrix was examined [18]. Recently, the shear band formation in MRE under stress relaxation has been reported by JOHARI et al. [19]. The correlation between the microstructural deformation and durability performance of MREs under stress relaxation was presented [20]. Most recently, the stress relaxations of isotropic and anisotropic MREs in the shear mode using single- and multi-step relaxation tests have been investigated by NAM et al. [21, 22].

The stress relaxation of viscoelastic polymeric materials can be examined numerically using fractional derivative viscoelastic models [21–23]. Fractional viscoelastic models (Maxwell, Kelvin–Voigt, Poynting–Thomson, Zener, etc.) have been constructed by the series and/or parallel combinations of elastic spring and fractional-order dashpot [24–26]. In fractional derivative viscoelastic models, the elastic spring is utilized to represent the time-independent elastic behavior, while the fractional-order dashpot is used to describe the time-dependent viscous response. Several fractional derivatives have been applied for viscoelastic models, such as the Riemann–Liouville derivative, the Caputo derivative, the Hadamard derivative, and fractional derivatives with the exponential function or the Mittag–Leffler function. The Mittag–Leffler function was considered to be a general empirical law for both creep and relaxation functions [27, 28]. Besides, GUO et al. [23] showed that the Mittag–Leffler function is applicable for fitting the measured data of stress relaxation of polyurethane foams.

In our previous studies [21, 22], four-parameter fractional Zener and Poynting–Thomson viscoelastic models were applied to describe the stress relaxation behavior of MREs. The stress relaxation response of the isotropic MRE was examined by single- and multi-step relaxation tests in a shear mode using double-lap shear specimens. For this study, numerical simulations of single- and multi-step shear stress relaxations of the isotropic MRE were investigated using the simplest fractional derivative viscoelastic models with only three parameters, namely fractional Maxwell model (FMM) and fractional Kelvin–Voigt model (FKM). The model parameters were determined by fitting the short-term experimental data and were used to predict the long-term stress relaxation of the isotropic MRE. The maximal difference between model fitted and measured data was presented to indicate the most suitable model for depicting the stress relaxation of the isotropic MRE.

2. Materials and methods

2.1. Materials

The isotropic MRE is fabricated from micro-sized CIPs, silicone rubber ZA13, and its catalyst. The silicone rubber ZA13 and its catalyst are produced by Zhermack S.P.A (Italy) and are supplied by Havel Composites Ltd. (Czech Republic). The micro-sized CIPs (type: 44890) provided by Sigma-Aldrich (USA) have a purity of 99.5% and a density of 7.86 g/cm^3. The grain size of the CIPs is between 5 and 9 µm. The microstructural morphology of the CIPs and their diameter as a function of the volume fraction in overall distribution can be found in our earlier article [29].

The fabrication of the isotropic MRE is described as follows. At first, the silicone rubber ZA13 was mixed with its catalyst in a mass ratio of 1:1. Subsequently, the micro-sized CIPs with a volume fraction of 27% were added to the mixture. Next, the mixture was well stirred in a glass cup and then placed in a vacuum chamber for about 15 min to remove air bubbles trapped inside the material during the mixing process. Afterward, the mixture was filled into a plastic mold and was put in the vacuum chamber for about 10 min to eliminate thoroughly the air bubbles trapped inside the mixture. Finally, the mixture in the mold was cured overnight at room temperature (RT) in the chamber while the vacuum pump was turned off to obtain the isotropic MRE. Microstructural morphologies of the isotropic MRE can be found in our earlier report [29].

2.2. Stress relaxation measurements

The shear stress relaxation of the isotropic MRE was studied using single- and multi-step relaxation tests. The stress relaxation tests were conducted for double-lap shear MRE samples at various constant strains (5, 10, 15, and 20%) with the magnetic flux density (MFD) changing from zero to 0.58 T using an Instron Electropuls testing system. The shear test, MRE double-lap sample, and electromagnet system were depicted in our earlier papers [21, 22, 29]. In the single- and multi-step relaxation tests, a strain rate of 1.0/s was applied in loading and unloading paths. The stress relaxation was recorded for 1000 s in the single-step relaxation test and 600 s for each step of the multi-step relaxation test. Shear strain-time curves of the isotropic MRE in the single- and multi-step relaxation tests are presented in Fig. 1. In the single-step relaxation test, a constant shear strain ε_0 is applied, and the stress $\sigma(t)$ is measured. The relaxation modulus is estimated using the formulation $G(t) = \sigma(t)/\varepsilon_0$. The measured results of the stress relaxation for the isotropic MRE are presented along with the numerical simulation results.
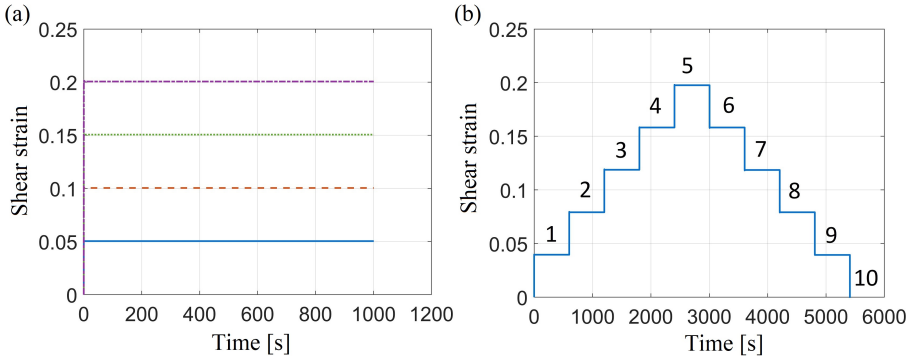
Fig. 1. Applied constant shear strains in (a) single- and (b) multi-step relaxation tests.

3. Fractional derivative viscoelastic models

The simplest fractional derivative viscoelastic models FMM and FKM were used to deal with the stress relaxation behavior of the isotropic MRE. These models were built by the series and/or parallel combinations of elastic spring and fractional-order dashpot. Figure 2 shows the single-element FMM and FKM.
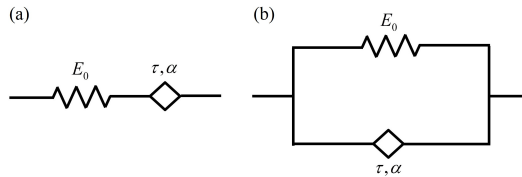

Fig. 2. Fractional derivative viscoelastic models: (a) FMM, (b) FKM.

The constitutive equations for the FMM and FKM in the time domain, respectively, are written as follows [25]:

$$(3.1) \qquad \frac{d^\alpha \sigma}{dt^\alpha} + \frac{\sigma}{\tau^\alpha} = E_0 \frac{d^\alpha \varepsilon}{dt^\alpha},$$

$$(3.2) \qquad \frac{d^\alpha \varepsilon}{dt^\alpha} + \frac{\varepsilon}{\tau^\alpha} = \frac{\sigma}{E_0 \tau^\alpha},$$

where E_0 is the elastic moduli of the springs, τ is the relaxation time of the fractional dashpot, and α is the fractional order with values varying between 0 and 1 [25].

The Riemann–Liouville (RL) fractional derivative was applied to the FMM and FKM to determine the stress relaxation functions. The RL fractional deriva-

tive is defined as [24]:

$$(3.3) \qquad {}^{RL}D^\alpha f(t) = \frac{d^\alpha f(t)}{dt^\alpha} = \frac{1}{\Gamma(1-\alpha)} \frac{d}{dt} \int_0^t \frac{f(s)}{(t-s)^\alpha} \, ds,$$

where Γ is the Eulerian Gamma function.

The Laplace transform of the fractional derivative of the order α is given by the following equation if the function $f(t)$ vanishes at $t = 0$ [27]:

$$(3.4) \qquad L\{D^\alpha f(t); s\} = s^\alpha \tilde{f}(s),$$

where $\tilde{f}(s)$ is the transform function of $f(t)$.

Applying the Laplace transform to Eq. (3.1) yields the following relationship:

$$(3.5) \qquad \tilde{\sigma}(s) = \frac{E_0 s^\alpha}{s^\alpha + \frac{1}{\tau^\alpha}} \tilde{\varepsilon}(s).$$

The Laplace transform of the relaxation modulus of the FMM can be derived as [28, 30]:

$$(3.6) \qquad \tilde{G}(s) = \frac{\tilde{\sigma}(s)}{s\tilde{\varepsilon}(s)} = E_0 \frac{s^{\alpha-1}}{s^\alpha + \frac{1}{\tau^\alpha}}.$$

Setting $\varepsilon = \varepsilon_0$ and taking the inverse Laplace transform to Eq. (3.6), the relaxation modulus of the FMM with Mittag–Leffler function kernel is obtained as [28]:

$$(3.7) \qquad G_{FMM}(t) = E_0 M_\alpha \left(-\left(\frac{t}{\tau}\right)^\alpha \right),$$

where $M_\alpha(x)$ is the single parameter Mittag–Leffler function and is defined as [31]:

$$(3.8) \qquad M_\alpha(x) = \sum_{n=0}^{\infty} \frac{x^n}{\Gamma(1+\alpha n)}.$$

Using the same procedure of FMM leads to the relaxation modulus of FKM as follows [28]:

$$(3.9) \qquad G_{FKM}(t) = E_0\left(1 + \frac{(t/\tau)^{-\alpha}}{\Gamma(1-\alpha)}\right).$$

4. Numerical simulation results and comparison with measured data

4.1. Single-step stress relaxation results

The FMM and FKM were applied to study the single- and multi-step stress relaxations of the isotropic MRE. Equations (3.7) and (3.9) were used to fit the relaxation modulus measured by the single- and multi-step relaxation tests. The fitting was done using the nonlinear least-squares method in Matlab. The values of the Mittag-Leffler function were computed according to an optimal parabolic contour (OPC) algorithm described by Garrappa [32]. The OPC method allowed the efficient calculation of the Mittag-Leffler function with high accuracy based on the numerical inversion of its Laplace transform. The parameters of the models FMM and FKM fitted with the experimental data of the single-step stress relaxation for the isotropic MRE at various constant strains are given in Table 1. The fitted and experimental relaxation moduli at different constant strains are presented in Fig. 3. A comparison of calculated and experimental shear stress at various constant strains for the isotropic MRE is depicted in Fig. 4.

Table 1. Fitting parameters of FMM and FKM to single-step stress relaxation data for the isotropic MRE.

Constant strain	FMM			FKM		
	E_0 [MPa]	α	τ [s]	E_0 [MPa]	α	τ [s]
0.05	1.92	0.052	4.61E-09	0.359	0.224	3.96E-02
0.10	1.79	0.051	6.73E-09	0.357	0.230	3.35E-02
0.15	1.79	0.051	4.95E-09	0.353	0.240	3.94E-02
0.20	1.73	0.050	6.01E-09	0.353	0.257	4.85E-02

It is clear from Table 1 that with the increase of the constant strain in the FMM, the parameter E_0 decreases slightly, while the fractional order α is nearly unchanged. For the FKM, although the fractional order increases with increasing the constant strain, the parameter E_0 changes slightly. Compared to the FKM, the FMM shows a much higher parameter E_0 and significantly lower fractional order α and the relaxation time τ as well. The parameter τ of the models describes the time at which the transition is centered for the relaxation modulus [21]. The fractional order α represents the distribution of stress relaxation processes [22]. Hence, it has a significant physical interpretation. A smaller α shows that materials have a broad distribution of stress relaxation processes. The results in Table 1 indicated that the FMM exhibits a more pronounced elastic property and less viscous characteristic than the FKM.

Besides, the maximal differences between the measured and fitted relaxation moduli of the FMM and FKM are 5.23% and 0.69%, respectively. Therefore, fitting the relaxation modulus of the FMM to measured data is less accurate
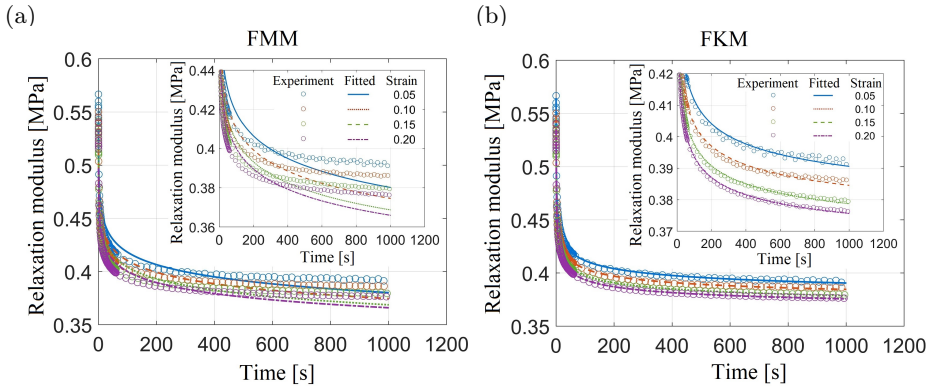
Fig. 3. Relaxation modulus (experimental and model fitted curves) of the isotropic MRE at different constant strains in the single-step stress relaxation. The insets are the zooms of the relaxation modulus.
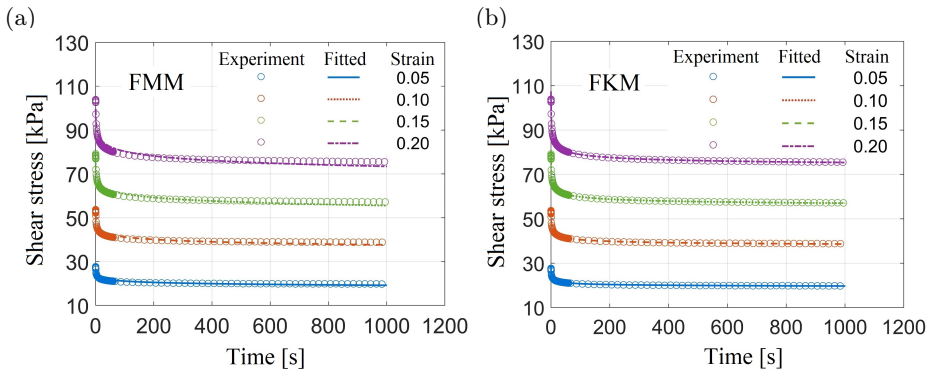

Fig. 4. Shear stress (experimental and calculated curves) of the isotropic MRE at different constant strains in the single-step stress relaxation.

than that of the FKM (see Fig. 3). The less accuracy of the fitting relaxation modulus of the FMM is attributable to a much smaller fractional order and the extremely short relaxation time of the FMM. The comparison between measured and estimated shear stresses in Fig. 4 also indicates a better agreement of the FKM than the FMM. The maximal differences between measured and calculated stresses of the FMM and FKM are 4.39% and 1.23%, respectively.

Moreover, the single-step stress relaxation of the isotropic MRE under different MFDs was numerically investigated using the FMM and FKM. The parameters of the FMM and FKM fitted to the experimental data of the single-step stress relaxation at various constant strains under different MFDs are given in Tables 2 and 3. The fittings of the relaxation modulus to the measured data at the constant strain of 20% under various MFDs for the isotropic MRE in the

single-step stress relaxation are presented in Fig. 5. The comparison between measured shear stresses of the isotropic MRE in the single-step relaxation and calculated stresses with long-term predictions over time using the investigated models is described in Fig. 6.

As Tables 2 and 3 show, although the fractional parameter α has an uneven change with raising the MFD, the parameter E_0 enhances with increasing the MFD to about 0.5 T and then changes slightly above 0.5 T. The variation of

Table 2. Fitting parameters of the FMM to the measured data of the single-step relaxation test for the isotropic MRE.

Strain	Parameter	MFD [T]				
		0.201	0.373	0.478	0.538	0.58
0.05	E_0 [MPa]	1.975	2.072	2.199	2.210	2.231
	α	0.052	0.051	0.052	0.051	0.052
	τ [s]	4.81E-09	4.45E-09	6.03E-09	4.75E-09	7.69E-09
0.10	E_0 [MPa]	1.836	1.961	1.995	2.085	2.093
	α	0.049	0.050	0.050	0.051	0.051
	τ [s]	4.51E-09	4.34E-09	7.38E-09	4.25E-09	4.78E-09
0.15	E_0 [MPa]	1.867	1.917	1.988	2.020	2.002
	α	0.051	0.050	0.051	0.051	0.051
	τ [s]	4.55E-09	6.75E-09	6.69E-09	4.64E-09	7.49E-09
0.20	E_0 [MPa]	1.729	1.745	1.787	1.856	1.846
	α	0.047	0.045	0.046	0.047	0.047
	τ [s]	6.65E-09	4.54E-09	5.51E-09	3.45E-09	4.87E-09

Table 3. Fitting parameters of the FKM to the measured data of the single-step relaxation test for the isotropic MRE.

Strain	Parameter	MFD [T]				
		0.201	0.373	0.478	0.538	0.58
0.05	E_0 [MPa]	0.376	0.407	0.427	0.430	0.426
	α	0.237	0.249	0.253	0.245	0.228
	τ [s]	4.37E-02	4.94E-02	4.73E-02	4.79E-02	4.79E-02
0.10	E_0 [MPa]	0.376	0.400	0.405	0.409	0.416
	α	0.250	0.268	0.252	0.247	0.239
	τ [s]	3.58E-02	3.89E-02	3.93E-02	4.02E-02	3.70E-02
0.15	E_0 [MPa]	0.364	0.382	0.393	0.398	0.400
	α	0.242	0.243	0.247	0.248	0.242
	τ [s]	3.95E-02	3.30E-02	4.33E-02	4.12E-02	3.97E-02
0.20	E_0 [MPa]	0.371	0.395	0.401	0.403	0.405
	α	0.259	0.298	0.286	0.283	0.283
	τ [s]	3.94E-02	4.66E-02	4.60E-02	4.33E-02	4.27E-02

the parameter E_0 with the rise in the MFD is similar to the change of the relaxation modulus and shear stress of the isotropic MRE (see Figs. 5 and 6). This change can be explained by the fact that the CIPs in the isotropic MRE under magnetic fields tend to move closer, leading to increasing the interaction between them, thereby enhancing the strength and stiffness of the isotropic MRE [21]. Besides, the rise in the relaxation modulus with raising the MFD is ascribable to increasing the MR effect of the isotropic MRE [29]. However, the relaxation modulus and shear stress grow slightly with the rise of the MFD above 0.5 T. This result indicates that the gain in the relaxation modulus and shear stress is limited even though the MFD is increased because the solid-like behavior of the isotropic MRE restricted the movement of CIPs under high MFDs.

As described above, the FMM shows a much greater parameter E_0 and lower fractional order α than the FKM. The MREs with smaller α values need a broad
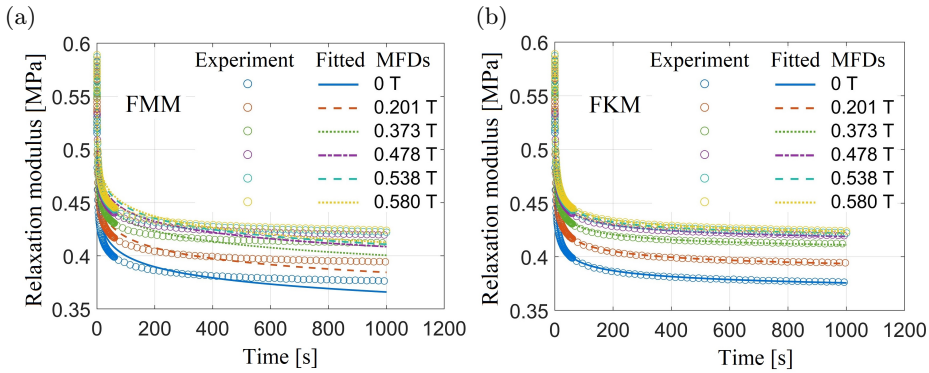

FIG. 5. Relaxation modulus (experimental and model fitted curves) of the isotropic MRE at the constant strain of 20% under different MFDs in the single-step stress relaxation.
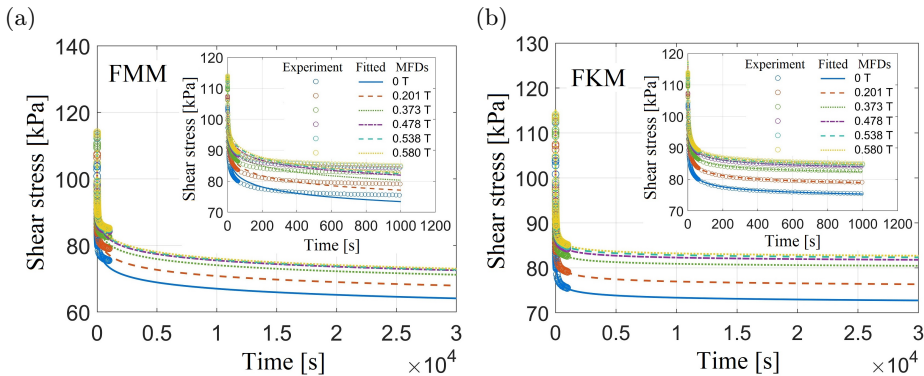

FIG. 6. Shear stress (experimental and model fitted curves) of the isotropic MRE at the constant strain of 20% under different MFDs in the single-step stress relaxation. The insert is a zoom of the first 1000 s.

distribution of relaxation time [21, 22]. Besides, fitting the relaxation modulus of the FKM to the experimental data is more accurate than that of the FMM (see Fig. 5). Moreover, the comparison between experimental and calculated stresses with long-term predictions in Fig. 6 also shows a better agreement of the FKM than the FMM. The maximal differences between the measured and estimated curves of the relaxation modulus and shear stress of the FMM and FKM are 6.32% and 5.37%, and 1.07% and 1.29%, respectively. Generally, the FKM with only three parameters was fitted well with the measured data of the single-step relaxation test for the isotropic MRE. This model can be used to predict the long-term single-step relaxation of the isotropic MRE.

4.2. Multi-step stress relaxation results

The multi-step stress relaxation behavior of the isotropic MRE was described using the FMM and FKM. The fittings of the FMM and FKM to the measured results in the multi-step relaxation test were done using the nonlinear least-squares method in Matlab. The parameters of studied models obtained from the fittings of the multi-step relaxation modulus to the experimental data are given in Tables 4 and 5. The models fitted relaxation modulus compared to the measured data of the isotropic MRE sample under various MFDs in the multi-

Table 4. Fitting parameters of the FMM to the measured data of the multi-step relaxation test for the isotropic MRE.

MFD [T]	Parameters	Steps								
		1	2	3	4	5	6	7	8	9
0	E_0 [MPa]	1.712	1.202	1.045	0.986	0.969	1.457	1.559	1.705	2.193
	α	0.047	0.030	0.023	0.021	0.023	0.009	0.013	0.018	0.031
	τ [s]	5.90E-09	1.18E-08	3.81E-08	2.68E-07	3.48E-06	2.86E-08	2.53E-08	2.32E-08	9.56E-09
0.201	E_0 [MPa]	1.752	1.257	1.097	1.019	0.997	1.461	1.565	1.752	2.328
	α	0.047	0.031	0.024	0.021	0.022	0.010	0.013	0.019	0.034
	τ [s]	1.04E-08	1.31E-08	2.22E-08	8.06E-08	9.79E-07	2.71E-08	1.01E-08	2.04E-08	1.01E-08
0.373	E_0 [MPa]	1.976	1.381	1.177	1.093	1.074	1.460	1.599	1.798	2.437
	α	0.050	0.033	0.026	0.022	0.022	0.011	0.015	0.020	0.034
	τ [s]	4.62E-09	1.09E-08	1.87E-08	2.16E-08	5.20E-08	2.23E-08	1.97E-08	1.73E-08	1.06E-08
0.478	E_0 [MPa]	2.129	1.448	1.231	1.131	1.100	1.465	1.612	1.845	2.552
	α	0.053	0.035	0.027	0.023	0.022	0.012	0.016	0.022	0.035
	τ [s]	6.53E-09	1.14E-08	1.25E-08	1.94E-08	3.41E-08	1.98E-08	2.61E-08	1.57E-08	1.11E-08
0.538	E_0 [MPa]	2.139	1.462	1.228	1.121	1.084	1.465	1.612	1.865	2.625
	α	0.052	0.036	0.027	0.022	0.021	0.012	0.016	0.022	0.036
	τ [s]	5.66E-09	1.96E-08	2.02E-08	2.56E-08	1.10E-07	1.88E-08	2.43E-08	1.70E-08	1.01E-08
0.580	E_0 [MPa]	2.105	1.487	1.249	1.128	1.078	1.455	1.594	1.864	2.616
	α	0.052	0.036	0.027	0.022	0.021	0.012	0.015	0.022	0.035
	τ [s]	8.57E-09	1.25E-08	2.08E-08	3.82E-08	1.85E-07	1.97E-08	1.23E-08	1.24E-08	1.01E-08

Table 5. Fitting parameters of the FKM to the measured data of the multi-step relaxation test for the isotropic MRE.

MFD [T]	Parameters	Steps								
		1	2	3	4	5	6	7	8	9
0	E_0 [MPa]	0.359	0.362	0.363	0.350	0.328	0.359	0.353	0.351	0.364
	α	0.226	0.196	0.186	0.127	0.084	0.282	0.216	0.199	0.192
	τ [s]	5.11E-02	1.37E-03	1.62E-04	3.36E-06	2.91E-07	5.73E-04	2.93E-04	1.16E-03	3.27E-02
0.201	E_0 [MPa]	0.374	0.375	0.374	0.370	0.359	0.365	0.355	0.346	0.348
	α	0.230	0.211	0.208	0.175	0.132	0.311	0.244	0.220	0.202
	τ [s]	5.50E-02	2.74E-03	5.32E-04	5.14E-05	5.61E-06	1.76E-03	1.11E-03	3.70E-03	8.44E-02
0.373	E_0 [MPa]	0.385	0.379	0.381	0.374	0.359	0.374	0.359	0.346	0.319
	α	0.220	0.168	0.165	0.139	0.102	0.288	0.221	0.205	0.195
	τ [s]	7.54E-02	1.53E-03	1.59E-04	1.17E-05	9.50E-07	1.05E-03	6.81E-04	3.46E-03	1.48E-01
0.478	E_0 [MPa]	0.380	0.375	0.381	0.388	0.374	0.382	0.365	0.348	0.315
	α	0.199	0.166	0.147	0.146	0.117	0.271	0.210	0.195	0.186
	τ [s]	1.05E-01	1.45E-03	1.10E-04	6.25E-05	2.34E-06	8.00E-04	6.29E-04	3.86E-03	2.35E-01
0.538	E_0 [MPa]	0.383	0.392	0.382	0.391	0.383	0.385	0.366	0.339	0.297
	α	0.197	0.185	0.154	0.140	0.121	0.268	0.219	0.223	0.210
	τ [s]	9.69E-02	4.03E-03	8.11E-05	2.33E-05	1.95E-06	7.47E-04	8.70E-04	1.04E-02	4.30E-01
0.580	E_0 [MPa]	0.394	0.380	0.376	0.387	0.386	0.386	0.366	0.341	0.298
	α	0.208	0.145	0.140	0.123	0.125	0.283	0.227	0.206	0.184
	τ [s]	9.04E-02	1.64E-03	4.78E-05	1.34E-05	2.17E-06	1.12E-03	1.12E-03	5.73E-03	3.41E-01

step stress relaxation test is presented in Fig. 7. Besides, the shear stress of the isotropic MRE as a function of time under different MFDs was calculated using the investigated models with the fitted parameters. The predicted shear stresses of the studied models compared to the measured data of the MRE samples under various MFDs are shown in Fig. 8.

As observed in Table 4, although the parameters E_0 and α of the FMM enhance moderately with increasing the MFD, they decrease considerably with time in the loading path and increase in the unloading path. Besides, results in Table 4 show extremely short relaxation time τ of the FMM. For the FKM, with the rise of the MFD, the parameter E_0 tends to a slight increase while the fractional order α varies irregularly (Table 5). However, the parameter E_0 changes slightly with the MFDs above 0.5 T, as presented above. Moreover, the parameter E_0 of the FKM varies lightly with time, whereas the fractional order α decreases over time in both loading and unloading paths.

The shear stress and modulus of the isotropic MRE reduce during the relaxation periods in the loading path, while they enhance during the relaxation segments in the unloading path (Figs. 7 and 8). Besides, results in Figs. 7 and 8 revealed that the stress relaxation behavior of the MRE depends on the applied magnetic field in the multi-step relaxation test. The relaxation modulus and shear stress in the loading path of the multi-step relaxation increase sig-

nificantly with increasing the MFD to about 0.5 T and enhance slightly above 0.5 T, as described in the single-step relaxation part. Moreover, with the rise in the MFD, the shear stress and relaxation modulus at steps 6 and 7 in the unloading path behave similarly to those in the loading path. Nevertheless, the relaxation modulus and shear stress at steps 8 and 9 change in reverse with increasing the MFD. This change can be explained that the MRE sample temperature is enhanced by raising the magnetic field intensity of the electromagnet [21, 22].

Moreover, results in Fig. 7 indicated that the fitting of the relaxation modulus of the FMM to the experimental data of multi-step relaxation test under different MFDs is less precise than that of the FKM. Therefore, the agreement between measured and estimated shear stresses with long-term predictions of the FKM is better than that of the FMM (see Fig. 8). The fitting of the FKM is accurate for all strain steps under the MFDs in the loading and unloading paths of the multi-step stress relaxation test for the isotropic MRE. The maximal differences between the measured and predicted curves of the FMM and FKM for the isotropic MRE under various MFDs are 6.7% and 0.88%, respectively. In
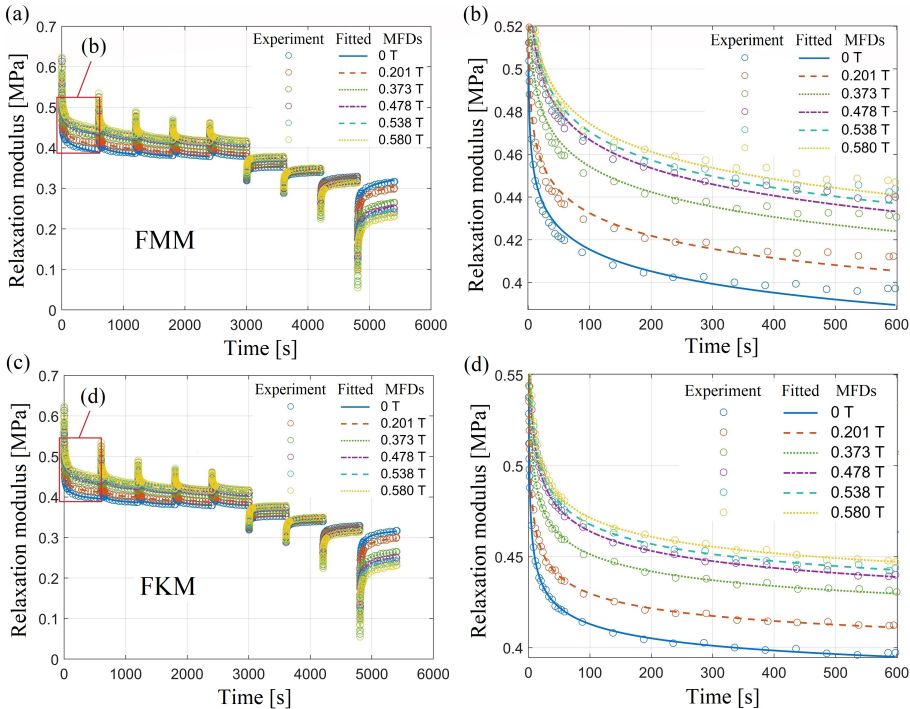

Fig. 7. Relaxation modulus (experimental and model fitted curves) of the isotropic MRE under different MFDs in the multi-step relaxation test.
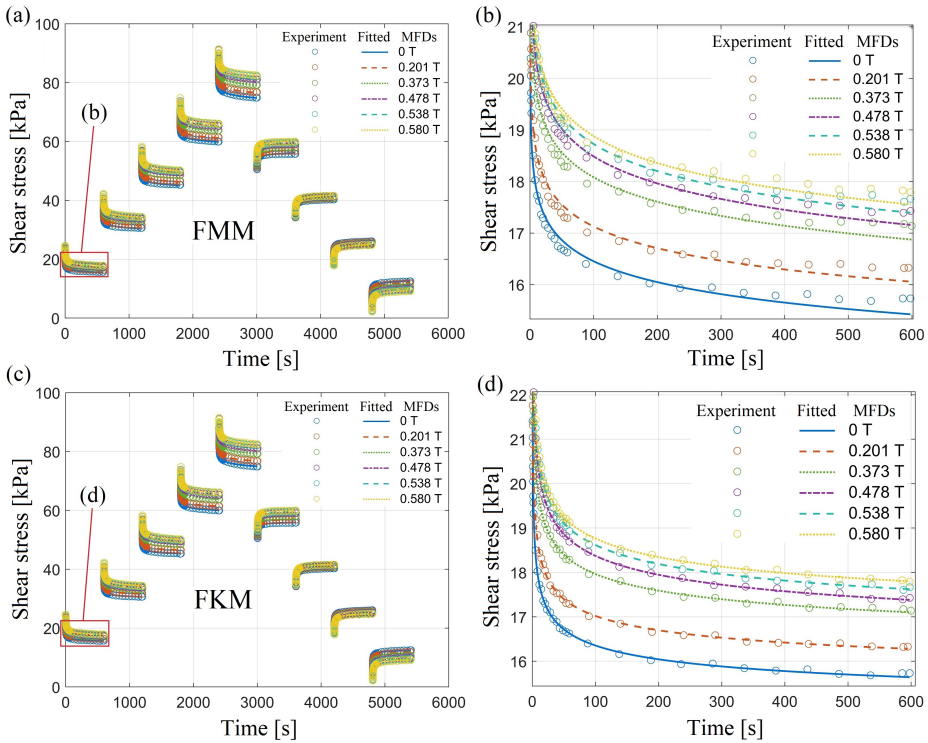
Fig. 8. Shear stress (experimental and model fitted curves) of the isotropic MRE under different MFDs in the multi-step relaxation test.

general, the numerically calculated results showed that the FKM is better than the FMM and can be applied to predict the multi-step stress relaxation of the isotropic MRE.

5. Conclusions

The numerical studies on the shear stress relaxation of isotropic MRE made of silicone rubber and micro-sized CIPs using the simplest fractional derivative viscoelastic models have been conducted in this paper. The fractional Maxwell and Kelvin–Voigt viscoelastic models were used to fit the experimental data of the isotropic MRE measured by single- and multi-step relaxation tests at different constant strains and external magnetic fields. The fractional Maxwell viscoelastic model indicated a relatively large difference between the measured and calculated data. The fractional Kelvin–Voigt model was fitted well to the experimental data of the isotropic MRE at various constant strains under different MFDs in both single- and multi-step stress relaxations. A great agreement

between experimental and fitted relaxation modulus of fractional Kelvin–Voigt viscoelastic model under different strain levels and MFDs was obtained. The estimated shear stress with long-term predictions using the fractional Kelvin–Voigt viscoelastic model for the isotropic MRE is in very good agreement with the measured one. In short, the fractional derivative Kelvin–Voigt viscoelastic model with only three parameters can be used to predict the long-term stress relaxation of the isotropic MRE.

Conflict of interest

The authors declare that they have no conflict of interest.

Acknowledgements

References

1. Z. Rigbi, L. Jilken, *The response of an elastomer filled with soft ferrite to mechanical and magnetic influences*, Journal of Magnetism and Magnetic Materials, **37**, 3, 267–276, 1983.

2. A.K. Bastola, *A review on magneto-mechanical characterizations of magnetorheological elastomers*, Composites Part B: Engineering, **200**, 108348, 2020.

3. A.G. Díez, C.R. Tubio, J.G. Etxebarria, S. Lanceros-Mendez, *Magnetorheological elastomer-based materials and devices: state of the art and future perspectives*, Advanced Engineering Materials, **23**, 6, 2100240, 2021.

4. H.X. Deng, X.L. Gong, *Application of magnetorheological elastomer to vibration absorber*, Communications in Nonlinear Science and Numerical Simulation, **13**, 1938–1947, 2008.

5. P. Gao, H. Liu, C. Xiang, P. Yan, T. Mahmoud, *A new magnetorheological elastomer torsional vibration absorber: structural design and performance test*, Mechanical Sciences, **12**, 1, 321–332, 2021.

6. A.K. Bastola, L. Li, *A new type of vibration isolator based on magnetorheological elastomer*, Materials & Design, **157**, 431–436, 2018.

7. S. Liu, L. Feng, D. Zhao, X. Shi, Y. Zhang, J. Jiang, et al., *A real-time controllable electromagnetic vibration isolator based on magnetorheological elastomer with quasi-zero stiffness characteristic*, Smart Materials and Structures, **28**, 8, 085037, 2019.

8. T. Hu, S. Xuan, L. Ding, X. Gong, *Stretchable and magneto-sensitive strain sensor based on silver nanowire-polyurethane sponge enhanced magnetorheological elastomer*, Materials & Design, **156**, 528–537, 2018.

9. H. Böse, T. Gerlach, J. Ehrlich, *Magnetorheological elastomers – An underestimated class of soft actuator materials*, Journal of Intelligent Material Systems and Structures, **32**, 14, 1550-1564, 2021.

10. I.L. Lapipo, J.D. Fadly, W.F. Faris, *Characterization of magnetorheological elastomer (MRE) engine mounts*, Materials Today: Proceedings, **3**, 411–418, 2016.

11. C. Wu, Q. Zhang, X. Fan, Y. Song, Q. Zheng, *Smart magnetorheological elastomer peristaltic pump*, Journal of Intelligent Material Systems and Structures, **30**, 7, 1084–1093, 2019.

12. M. Lapine, I.V. Shadrivov, D.A. Powell, Y.S. Kivshar, *Magnetoelastic metamaterials*, Nature Materials, **11**, 1, 30–33, 2012.

13. R.L. Harne, Y. Deng, M.J. Dapino, *Adaptive magnetoelastic metamaterials: A new class of magnetorheological elastomers*, Journal of Intelligent Material Systems and Structures, **29**, 2, 265–278, 2018.

14. A.K. Bastola, M. Hossain, *The shape–morphing performance of magnetoactive soft materials*, Materials & Design, **211**, 110172, 2021.

15. N. Bira, P. Dhagat, J.R. Davidson, *A review of magnetic elastomers and their role in soft robotics*, Frontiers in Robotics and AI, **7**, 146, 2020.

16. A.F.M.S. Amin, A. Lion, S. Sekita, Y. Okui, *Nonlinear dependence of viscosity in modeling the rate-dependent response of natural and high damping rubbers in compression and shear: experimental identification and numerical verification*, International Journal of Plasticity, **22**, 1610–1657, 2006.

17. L. Wang, Y. Han, *Compressive relaxation of the stress and resistance for carbon nanotube filled silicone rubber composite*, Composites Part A: Applied Science and Manufacturing, **47**, 63–71, 2013.

18. S. Qi, M. Yu, J. Fu, M. Zhu, *Stress relaxation behavior of magnetorheological elastomer: experimental and modeling study*, Journal of Intelligent Material Systems and Structures, **29**, 205–213, 2018.

19. M.A.F. Johari, S.A. Mazlan, N.A. Nordin, S.A.A. Aziz, N. Johari, N. Nazmi, K. Homma, *Shear band formation in magnetorheological elastomer under stress relaxation*, Smart Materials and Structures, **30**, 4, 045015, 2021.

20. M.A.F. Johari, S.A. Mazlan, M.M. Nasef, U. Ubaidillah, N.A. Nordin, S.A.A. Aziz, N. Johari, N. Nazmi, *Microstructural behavior of magnetorheological elastomer undergoing durability evaluation by stress relaxation*, Scientific Reports, **11**, 1, 1–17, 2021.

21. T.H. Nam, I. Petríková, B. Marvalová, *Experimental and numerical research of stress relaxation behavior of magnetorheological elastomer*, Polymer Testing, **93**, 106886, 2021.

22. T.H. Nam, I. Petríková, B. Marvalová, *Effects of loading rate, applied shear strain, and magnetic field on stress relaxation behavior of anisotropic magnetorheological elastomer*, Mechanics of Advanced Materials and Structures, **29**, 20, 2984–2998, 2022.

23. X. Guo, G. Yan, L. Benyahia, S. Sahraoui, *Fitting stress relaxation experiments with fractional Zener model to predict high frequency moduli of polymeric acoustic foams*, Mechanics of Time-Dependent Materials, **20**, 4, 523–533, 2016.

24. T.A. Nadzharyan, S.A. Kostrov, G.V. Stepanov, E.Y. Kramarenko, *Fractional rheological models of dynamic mechanical behavior of magnetoactive elastomers in magnetic fields*, Polymer, **142**, 316–329, 2018.

25. A. Bonfanti, J.L. Kaplan, G. Charras, A. Kabla, *Fractional viscoelastic models for power-law materials*, Soft Matter, **16**, 26, 6002–6020, 2020.

26. H. Xu, X. Jiang, *Creep constitutive models for viscoelastic materials based on fractional derivatives*, Computers & Mathematics with Applications, **73**, 6, 1377–1384, 2017.

27. F. Mainardi, *Fractional Calculus and Waves in Linear Viscoelasticity: an Introduction to Mathematical Models*, Imperial College Press, London, 2010.

28. F. Mainardi, G. Spada, *Creep, relaxation and viscosity properties for basic fractional models in rheology*, The European Physical Journal Special Topics, **193**, 1, 133–160, 2011.

29. T.H. Nam, I. Petríková, B. Marvalová, *Experimental characterization and viscoelastic modeling of isotropic and anisotropic magnetorheological elastomers*, Polymer Testing, **81**, 106272, 2020.

30. X. Su, W. Xu, W. Chen, H. Yang, *Fractional creep and relaxation models of viscoelastic materials via a non-Newtonian time-varying viscosity: physical interpretation*, Mechanics of Materials, **140**, 103222, 2020.

31. M. Niedziela, J. Wlazło, *Notes on computational aspects of the fractional-order viscoelastic model*, Journal of Engineering Mathematics, **108**, 1, 91–105, 2018.

32. R. Garrappa, *Numerical evaluation of two and three parameter Mittag–Leffler functions*, SIAM Journal of Numerical Analysis, **53**, 3, 1350–1369, 2015.